Engineering Conferences International
ECI Digital Archives

The 14th International Conference on Fluidization – From Fundamentals to Products

Refereed Proceedings

2013

Fluidization Regimes Characterized Using a Fast X-Ray Tomography Setup

Jean Saayman
University of Pretoria, South Africa

J. Ruud van Ommen
Delft University of Technology, Netherlands

Rob F. Mudde
Delft University of Technology, Netherlands

Evert C. Wagner
Delft University of Technology, Netherlands

Willie Nicol
University of Pretoria, South Africa

FLUIDIZATION REGIMES CHARACTERIZED USING A FAST X-RAY TOMOGRAPHY SETUP

Jean Saayman[1], J. Ruud van Ommen[2], Rob F. Mudde[2], Evert C. Wagner[2] and Willie Nicol[1]*
[1] *Department of Chemical Engineering, University of Pretoria, Main Campus, Corner Lynwood & Roper Street, Hatfield, Pretoria, 0002, South Africa*
[2] *Department of Chemical Engineering, Product and Process Engineering, Delft University of Technology, Julianalaan 136, 2628 BL Delft, The Netherlands*
** Corresponding author: Email - willie.nicol@up.ac.za; Tel - +2712 420 3796*

ABSTRACT
X-Ray Tomography (XRT) was applied to higher velocity regimes in order to non-intrusively measure cross-sectional solids concentration and observe flow structures of the bubbling-, turbulent- and fast fluidization regimes. It was confirmed that regime characterization can be done using pressure measurements, solids-fraction measurements and reconstructed tomography images.

INTRODUCTION
Gas-Solid fluidized beds are widely applied in industry. They have the advantages of good solids mixing, gas-solids contacting and low pressure drop relative to packed beds. Hydrodynamics and solid distribution are important for gas-solid contacting and in turn, reactor performance. Many techniques are employed to measure these properties pertaining to hydrodynamics, two of which being optical probes and tomography. Tomography is a useful and non-intrusive technique.

Ellis et al. (1) used optical probes with different column diameters and Geldart A Fluid Catalytic Cracking (FCC) catalyst to investigate the bubbling and turbulent regime. The voidage profile was asymmetrical close to the solids return inlet and bed surface; radial symmetry was observed for the rest of the bed. They reported some uncertainty due to the intrusive nature of the probes. Zhu et al. (2) installed three optical probes around the periphery of a fluidized bed at the same radial position. The bubbling and turbulent regime was investigated for FCC powder. No radial symmetry for the voidage profile was observed in the bubbling regime whereas symmetry did exist in the turbulent regime. Du et al. (3) used Electrical Capacitance Tomography (ECT) in conjunction with an optical probe to investigate bed non-homogeneity using FCC catalyst. They similarly found asymmetry for the bubbling regime and symmetry for turbulent. Also, the observation was made that ECT and the optical probes yield considerably different results in the void phase fraction depending on the signal's threshold level to distinguishing between emulsion and void phase. ECT is a fast and relatively inexpensive method of tomography and has been widely applied in recent years. A very comprehensive ECT study is that of Makkawi and Wright (4), which spanned several regimes for a shallow bed. The packed bed height and column diameter (13.8 cm) were equal to each other (5). ECT is, however, a soft-field technique, meaning that the gas-solid distribution influences the position of the field lines, resulting in relatively poor resolution at the centre of the bed (6). X-Ray Tomography (XRT) is a hard field technique: the direction of a field line is not changed by the medium. Recent advances in fast XRT makes it possible to implement time-resolved cross-sectional measuring in fluidized beds (7). These advances create the opportunity to measure three-dimensional bubble shapes; leading to new insight in bubble behaviour and cross sectional solids distribution. The XRT technique has proven useful for the

bubbling regime. Operating at higher velocities will result in faster hydrodynamics, different solids distributions and solids behaviour. It needs to be confirmed whether a fast XRT setup has sufficient temporal- and spatial resolution for measurements in these regimes.

The objective of this paper is to characterize the fluidization regime transitions using total cross-sectional solids distribution data obtained from non-intrusive X-ray measurements. The cross sectional solids concentration of the bubbling-, turbulent- and fast fluidization regimes will be investigated. The characteristics and dynamics of solids concentration in the different regimes will be compared to the ECT measurements of Makkawi and Wright (4) and the traditional quantification technique of pressure analysis.

EXPERIMENTAL

The investigation was conducted in an acrylic column 0.14 m in diameter and 1.4 m high. Two absolute-pressure sensors were installed, one in the plenum chamber and one 0.07 m from the distributor. Positioned around the column were 3 X-ray sources. Opposite to each X-ray source was a detector array; each array has a top and bottom row of 32 detectors, creating 64 lines of measurement through the column per source. This arrangement results in two measuring planes separated by approximately 10 mm. All 192 detectors record at a rate of 2500Hz. The basic setup is the same as the one used by Mudde (7,8), with the exception of a smaller column and source circle diameter. For more details on the setup and X-ray physics, please refer to these articles. At a specific superficial velocity and measuring height signals were logged for 300 seconds; Makkawi and Wright (5) recommend at least 120 seconds. The column was filled with sand, having a Sauter mean diameter of 101 µm and a solids density of 2530 kg/m^3, to a static bed height of 0.50 m. The achievable velocity range of the setup was 0.11 m/s up to 2.6 m/s. Four measuring heights above the distributor were investigated: 0.20 m, 0.30 m, 0.40 m and 0.50 m. The amount of solids missing on each line of measurement relative to a packed bed can be determined, which can easily be translated to a line solids fraction (φ_i). To do this calculation a calibration curve for each individual detector is required. Calibration points are determined by placing a thin acrylic partition in the column at different positions and filling one side with material. Using the following calibration function, A_{cal}, B_{cal} and C_{cal} can be determined for each individual detector:

$$I_{Xray} = A_{cal} + B_{cal} \exp\left({}^{-x}/_{C_{cal}}\right)$$

where, I_{xray} is the beam intensity and x is the amount of material between the source and detector. A weighted average between al 32 lines is calculated to obtain a cross-sectional solids fraction (φ). The weighting factor is based on each detector's line length (l_i) going through the bed. And average is taken between the values obtained from each detector-source pair:

$$\phi = \frac{1}{3}\left\{\left(\sum_{i=1}^{32}\frac{l_i}{l_T}\phi_i\right)_{source1} + \left(\sum_{i=1}^{32}\frac{l_i}{l_T}\phi_i\right)_{source2} + \left(\sum_{i=1}^{32}\frac{l_i}{l_T}\phi_i\right)_{source3}\right\}$$

where: $l_T = \sum_{i=1}^{32} l_i$

For these calculation 5 minutes of data was processed for both top and bottom measurement planes. Figure 1a illustrates the resulting cross-sectional solids concentration measurement. It can be seen as a void or possibly several voids move through the measurement plane a drop in solids concentration is observed. As the voids move upwards it goes through the bottom plane first and after some times through the top plane, which is observed in Figure 1a.

An average void rise velocity ($\bar{u}_v$) can be determined using the signals of both bottom and top planes. A similar method to the bubble linking algorithm of Rüdisüli et al. (9) is used. The Sum of Squared Differences (SSD) between the bottom and top plane can be calculated using both 5 minute signals. The whole top plane signal is then shifted in time until a minimum in the SSD is obtained. Figure 1 illustrates this technique: (a) is the original signals, (b) and (c) are the same signals, with the exception of the top plane signal being shifted in time. (d) shows the SSD as the top plane signal is shifted. **a**, **b** and **c** indicate the SSD of Figures 1a, 1b and 1c. The best agreement between the bottom and top signal is achieved at point **b.** At this time shift the SSD is at a minimum. This time shift value can be interpreted as the averaged time voids take to move from the bottom plane to the top plane. By knowing the distance between the two planes a velocity can be calculated ($\bar{u}_v$). Each bubble will have its own rise velocity depending on its size, $\bar{u}_v$ is however the time-averaged void rise velocity.

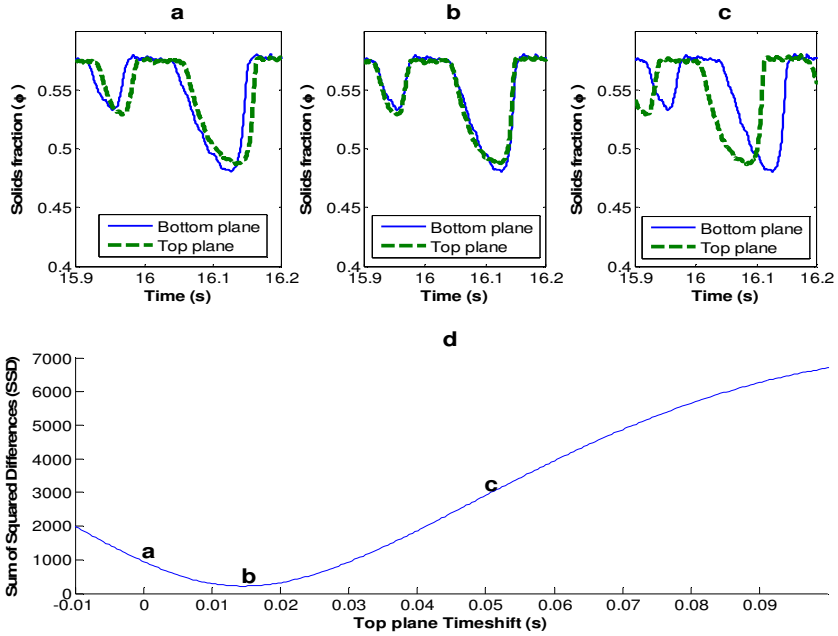

***Figure 1**: (a) is an example of the calculated cross sectional solids concentration signal obtained for both top and bottom measuring planes. The example is taken from the measurement done at 200mm above the distributor and at a velocity of 0.11 m/s. (b) and (c) shows the same signal, except the top plane's signal is shifted in time. (d) is the calculated SSD between the top and bottom plane signals at different top plane time shifts.*

RESULTS AND DISCUSSION

Pressure analysis

Using the standard deviation of pressure fluctuations the bubbling to turbulent transition (U_c) is determined to be 0.65 m/s and the end of turbulent fluidization (U_k) is at 1.19 m/s. The measurements were repeated three times and the average was calculated for each velocity. The standard deviation of pressure fluctuation with velocity is shown in Figure 2. Table 1 reports the top 4 Geldart B U_c-correlations according to Arnaldos and Casal (10). Also reported are their individual predictions for this specific system. Pressure measurements in the plenum chamber and in the bed are used to calculate the coherence between the signals. The standard deviation of the incoherent part of the pressure signal is a measure of void sizes

(11). It can be seen that the voids grow as the superficial velocity is increased in the bubbling regime and reach a maximum stable size in the turbulent regime. The sudden increase in the fast fluidization regime is due to the core-annulus structure which forms in the centre of the reactor.

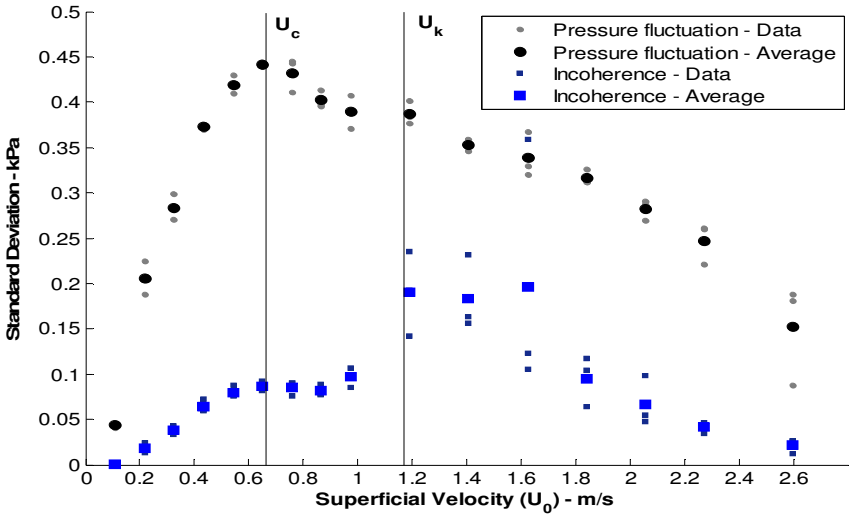

***Figure 2**: Standard deviation of pressure fluctuations, showing the bubbling to turbulent regime transition (U_c) occurs at 0.65 m/s. The end of turbulent fluidisation (U_k) is 1.19 m/s. Also shown is the standard deviation of incoherence, which is a measure of the void size.*

***Table 1**: U_c correlations and predictions (as quoted by Arnaldos & Casal (10)).*

Authors	Equation	Predicted value (m/s)
Jin et al. (12)	$u_c = (gd_p)^{0.5}[\frac{(KD_f)(\rho_s - \rho_g)}{d_p \rho_g}]^{0.27}$ $KD_f = 0.00367$ (for free bed)	0.66
Cai et al. (13)	$u_c = (gd_p)^{0.5}[\frac{0.211}{D_t^{0.27}} + \frac{2.42 \times 10^{-3}}{D_t^{1.27}}][\frac{D_t(\rho_s - \rho_g)}{d_p \rho_g}]^{0.27}$	0.68
Nakajima et al. (14)	$Re_c = 0.633Ar^{0.467}$	0.79
Lee and Kim (15)	$Re_c = 0.7Ar^{0.485}$	0.95

Solids concentration

Figure 3 shows the mean of the cross-sectional solids fraction ($\overline{\phi}$) obtained from the X-ray data for the bottom plane. Three distinct types of behaviour are observed which coincide with the different regimes. A sharp decrease with velocity can be seen in the bubbling regime and $\overline{\phi}$ decreases higher up in the reactor. Zhu et al. (2) observed similar height dependence using optical probes. The gradient of $\overline{\phi}$ changes for the turbulent regime; the same trend was seen by Makkawi and Wright (4) using ECT. What they could not observe however was effects higher up in the column, as they used a shallow bed. The solids concentrations levels off and remains fairly constant with velocity at 400 mm and 500 mm. At the highest gas velocity in the turbulent fluidization regime, solids concentration at 200 mm, 300 mm and 400 mm are the same. The solids concentration at 500 mm is lower. The packed bed height was 500 mm; therefore this measurement is close to the splash zone. The decreasing trend continues in the fast fluidization regime, as with the

bubbling regime. In the fast fluidization regime there is no difference with height, except for measurements at 500 mm, which is at the dense bed surface where one would expect lower $\overline{\phi}$. Pneumatic transport sets in at 2.60 m/s.

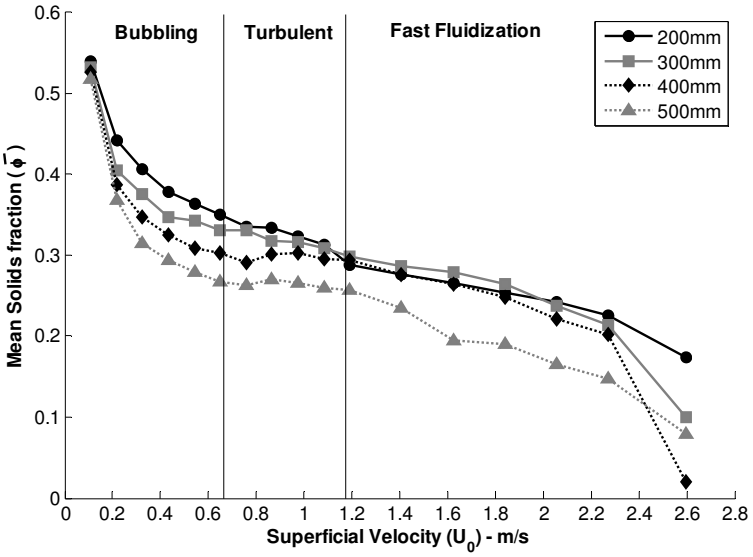

***Figure 3**: The average cross sectional voidage with superficial velocity at 200 mm, 300 mm, 400 mm and 500 mm from the distributor.*

To get an impression of the radial solids distribution the mean line solids fractions of each detector ($\overline{\phi_i}$) is shown for a single source in Figure 4. The values of the outer most detectors are not shown. Due to the close proximity of the detection line to the wall, column vibrations influenced the outer detector value. Between 0.65 m/s and 1.19 m/s the shape of the radial profiles are fairly constant with superficial velocity. Not only does $\overline{\phi}$ remain constant with superficial velocity, but the entire radial solids distribution as well. At the lowest superficial velocity asymmetry is observed, the asymmetry is due to low distributor pressure drop causing mal-distribution. At high velocities pressure drop across the distributor increases and better symmetry is observed. Slight deviation from symmetry is likely caused by the solids return. Ellis et al. (1) noted a similar effect due to the solids return. At 200 mm smooth profile contours are obtained for all velocities. Axially higher up in the column a spike in the radial centre is seen, which disappears as the fast fluidization regime is reached. It is not likely that this spike is due to mal-distribution since it is not observed at 200 mm, but due to bubble geometry. The bubble wake could cause this effect on a time average voidage signal. Bubbles were smaller lower down in the column which is why it is not seen at 200 mm, higher up bubbles merged and grew, moving up in the centre of the column.

Void behaviour and tomographic reconstructions

Figure 5 shows the result of the calculated average void rise velocity ($\bar{u}_v$). The particles are Geldart B particles. Bubble growth is to be expected and $\bar{u}_v$ should be a function of the bubble size. As the superficial velocity is increased into the turbulent regime the void rise velocity changes. For the bottom part of the column, at 200 mm, voids reach a constant velocity fairly quickly. This trend agrees well with the observed trend in the standard deviation of incoherence of Figure 2. The pressure probe was also in the bottom section of the column. Measurements higher up in the

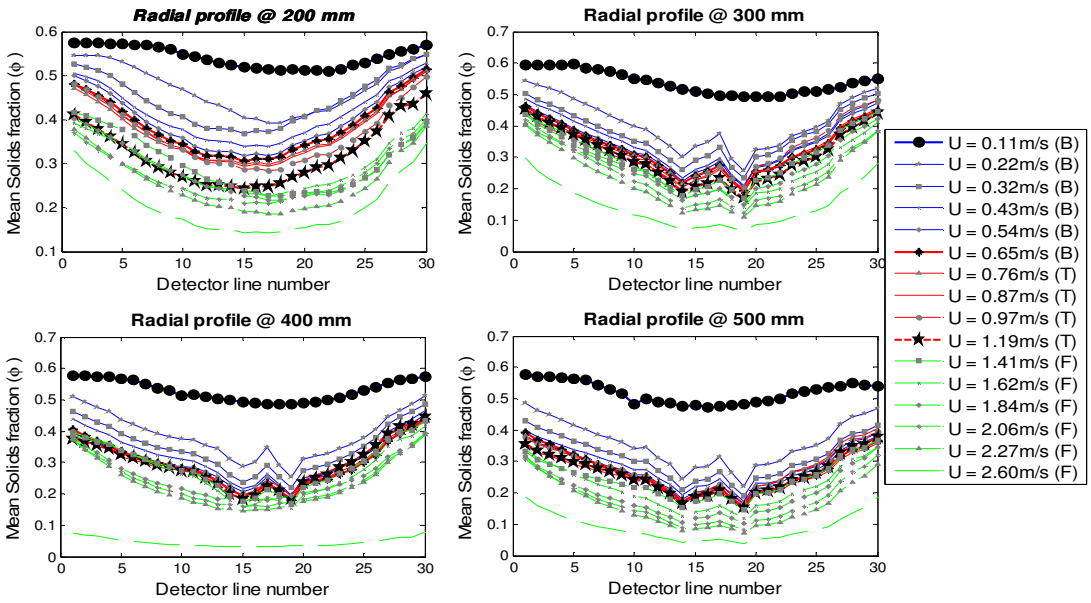

***Figure 4**: Radial solids distribution at different velocities and heights above the distributor. Indicated is the relevant regime at each velocity: "B" – bubbling regime, "T"-turbulent regime, "F" – fast fluidization regime.*

column all fall in a band where $\bar{u}_v$ levels off but does not necessarily reach a constant value. It seems even though cross sectional solids concentrations become independent of the superficial velocity in the turbulent regime, void dynamics does not. $\bar{u}_v$ in the fast fluidization regime had no clear trend and seemed to be random. These random values occur since there are no more distinct voids rising; rather a core-annulus structure forms, which fluctuates causing random minimums in the SSD's.

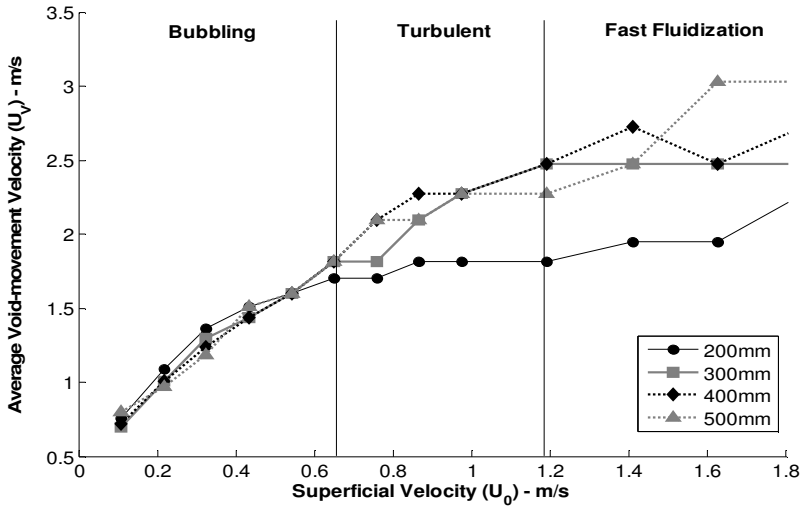

***Figure 5**: Average void movement.*

Two seconds of raw data for the bottom plane of sensors was processed using an iterative algebraic reconstruction algorithm. Signal noise, inherent to the X-Ray sensors, was eliminated by averaging over 10 samples. 55 by 55 pixel images were reconstructed. For more details on the reconstruction algorithm see previously

published work on the technique (6,8,16). The images were stacked and a pseudo-3D representation of bubbles/voids could be obtained. Figures 6 show the results for the bubbling regime (U_0 = 0.22 m/s), bubble-turbulent regime transition (U_0 = 0.65 m/s), turbulent regime (U_0 = 0.97 m/s) and fast fluidization regime (U_0 = 2.06 m/s). The z-axis is a time scale. Since the nose of a void will pass through the measurement plane first the time axis is inverted to ensure the pseudo-3D images are orientated correctly. Zero seconds being at the top and 2 seconds at the bottom. The bubbling-turbulent-transition is characterized with slug-like structures. This was also visually observed. Theory suggests that U_c is the point at which the largest stable bubbles exist, after U_c bubble breakup starts to dominate. In the turbulent regime a continuous train of bubbles are observed. This might be the start of a core annulus which momentarily collapses. A continuous uninterrupted void exists at 2.06 m/s, this is the core annulus which is characteristic of the fast fluidization regime.

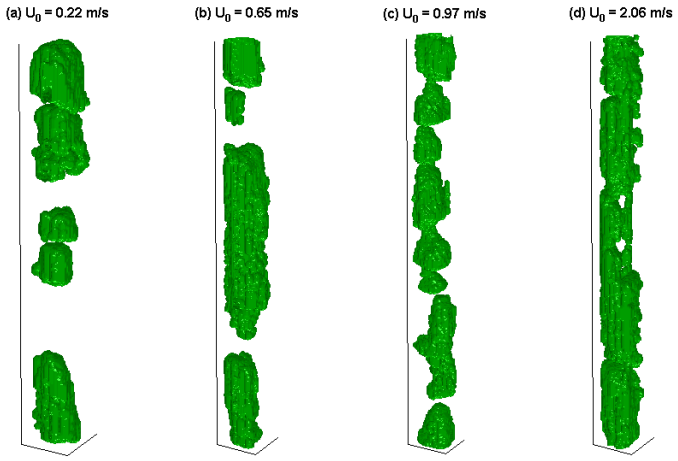

***Figure 6**: 3-D reconstruction of the void shapes at **400** mm above the distributor for the (a) bubbling regime, (b) bubble-turbulent regime transition, (c) turbulent regime and (d) fast fluidization regime.*

CONCLUSIONS

It was confirmed that regime characterization can be done using solids-fraction measurements and reconstructed flow structures obtained from a fast X-ray tomography setup. The setup had sufficient temporal and spatial resolution for the faster hydrodynamics of the higher velocity operating regimes, even more so the technique gave reliable and significantly more detailed results than ETC or optical probes. The bubbling- and fast fluidization- regimes' cross-sectional solids concentration visibly decreases with superficial velocity, whereas the turbulent regime is characterized with almost constant values. However, void dynamics does still change with superficial velocity in the turbulent regime. The fast fluidization regime's solids concentration is independent of axial height.

NOTATION

Ar	Archimedes number ($d_p^3.\rho_g.(\rho_s-\rho_g).g/\mu^2$)
A_{cal}	Calibration coefficient 1
B_{cal}	Calibration coefficient 2
C_{cal}	Calibration coefficient 3
d_p	Particle diameter (m)
D_t	Column Diameter (m)
g	Gravitational constant (m/s^2)
i	Xray beam number (-)
I_{Xray}	Xray beam intensity (au.)
l_i	Length of a single Xray beam inside the column (m)

l_T Total length of Xray beams in the column from a single source(m)
Re Reynolds number ($d_p.u_o.\rho_g/\mu$)
U_0 Operating superficial velocity (m/s)
U_c Turbulent transition velocity (m/s)
U_k End of turbulent regime (m/s)
$\bar{u}_v$ Average void rise velocity (m/s)
x Amount of material on between Xray source and detector (m)
ρ_g Gas density (kg/m^3)
ρ_s Solids density (kg/m^3)
μ Viscosity (Pa.s)
ϕ Instantaneous cross sectional solids fraction (-)
$\overline{\phi}$ Mean cross sectional solids fraction (-)
ϕ_i Instantaneous line solids fraction (-)
$\overline{\phi_i}$ Mean line solids fraction (-)

REFERENCES

(1) N. Ellis, H.T. Bi, C.J. Lim, J.R. Grace, Hydrodynamics of turbulent fluidized beds of different diameters, Powder Technology. 141 (2004) 124–136.
(2) H. Zhu, J. Zhu, G. Li, F. Li, Detailed measurements of flow structure inside a dense gas–solids fluidized bed, Powder Technology. 180 (2008) 339–349.
(3) B. Du, W. Warsito, L. Fan, Bed Nonhomogeneity in Turbulent Gas-Solid Fluidization, AIChE Journal. 49 (2003) 1110–1126.
(4) Y.T. Makkawi, P.C. Wright, Fluidization regimes in a conventional fluidized bed characterized by means of electrical capacitance tomography, Chemical Engineering Science. 57 (2002) 2411–2437.
(5) Y.T. Makkawi, P.C. Wright, Electrical capacitance tomography for conventional fluidized bed measurements—remarks on the measuring technique, Powder Technology. 148 (2004) 142–157.
(6) R.F. Mudde, Time-resolved X-ray tomography of a fluidized bed, Powder Technology. 199 (2010) 55–59.
(7) R.F. Mudde, Advanced measurement techniques for GLS reactors, The Canadian Journal of Chemical Engineering. 88 (2010) n/a–n/a.
(8) R.F. Mudde, Double X-ray Tomography of a Bubbling Fluidized Bed, Industrial & Engineering Chemistry Research. 49 (2010) 5061–5065.
(9) M. Rudisuli, T.J. Schildhauer, S.M. Biollaz, J.R. Van Ommen, Bubble characterization in a fluidized bed by means of optical probes, International Journal of Multiphase Flow. 41 (2012) 56–67.
(10) J. Arnaldos, J. Casal, Prediction of transition velocities and hydrodynamical regimes in fluidized beds, Powder Technology. 86 (1996) 285–298.
(11) J. Van der Schaaf, J.C. Schouten, F. Johnsson, C.M. Van den Bleek, Non-intrusive determination of bubble and slug length scales in fluidized beds by decomposition of the power spectral density of pressure time series, International Journal of Multiphase Flow. 28 (2002) 865–880.
(12) Y. Jin, Z.Q. Yu, Z. Wang, P. Cai, -, in: K. Østergaard, A. Sorensen (Eds.), Fluidization V, Engineering Foundation, New York, 1986: pp. 289–296.
(13) P. Cai, S.P. Chen, Y. Jin, Z.Q. Yu, Z.W. Wang, Effect of operating temperature and pressure on the transition from bubbling to turbulent fluidization, AIChE Symposium Series. 85 (1989) 37–43.
(14) M. Nakajima, M. Harada, M. Asai, R. Yamazaki, G. Jimbo, No Title, in: P. Basu, M. Horio, M. Hasatani (Eds.), Circulating Fluidized Bed Technology III, Pergamon, Oxford, 1991: pp. 79–84.
(15) G.S. Lee, S.D. Kim, Bed Expansion Characteristics and Transition Velocity in Turbulent Fluidized Beds, Powder Technology. 62 (1990) 207–215.
(16) R.F. Mudde, Bubbles in a Fluidized Bed : A Fast X-Ray Scanner, AIChE Journal. 57 (2011).